Karakoç, Alp; Hiltunen, Eero; Paltakari, Jouni

Geometrical and spatial effects on fiber network connectivity

Published in:
Composite Structures

DOI:
10.1016/j.compstruct.2017.02.062

Published: 15/05/2017

Document Version
Peer-reviewed accepted author manuscript, also known as Final accepted manuscript or Post-print

Please cite the original version:
Karakoç, A., Hiltunen, E., & Paltakari, J. (2017). Geometrical and spatial effects on fiber network connectivity. *Composite Structures*, *168*, 335-344. https://doi.org/10.1016/j.compstruct.2017.02.062

GEOMETRICAL AND SPATIAL EFFECTS ON FIBER NETWORK CONNECTIVITY

Alp Karakoç*[,1,2], Eero Hiltunen[1], Jouni Paltakari[1]

[1]Aalto University, School of Chemical Technology, Department of Forest Products Technology, P.O. Box 16300, FI-00076 AALTO, FINLAND

[2]University of California Los Angeles, Civil and Environmental Engineering, 90095, Los Angeles, CA, USA

ABSTRACT

For fibrous materials such as nonwoven fabrics, paper and paperboards, inter-fiber bonds play a critical role by holding fibers, thus providing internal cohesion. Being a physical phenomenon, inter-fiber bonds occur at every fiber crossing and can be also geometrically detected. In relation to the idea, a statistical geometrical model was developed to investigate the effects of fiber geometry, (i.e. length and cross-sectional properties), spatial distribution, (i.e. location and orientation), and specimen size on fiber network connectivity, which refers to inter-fiber bonds at fiber crossings. In order to generate the fiber network, a geometrical fiber deposition technique was coded in Mathematica technical computing software, which is based on the planar projections and intersections of fibers and provided as supplementary material to the present article. According to this technique, fiber geometries in discrete rectangular prismatic segments were generated by using uniform distributions of the geometrical and spatial parameters and projected onto the transverse plane. Then, projected geometries were trimmed within the transverse boundaries of the specified specimen shape, rectangular prism in this particular study. After this step, fiber crossings were determined through a search algorithm, which was also used as the basis for the fiber spatial regeneration. Thereafter, fibers were accumulated on top of each other by taking fiber crossings into account and eventually fiber networks based on selected properties were formed. By means of the proposed technique, a series of simulation experiments were conducted on paper fiber networks to investigate the correlation between the fiber network connectivity and fiber length, cross-sectional properties, orientation and specimen length, width and thickness.

Keywords: A. Fibers; A. Layered structures; B. Microstructures; C. Computational modelling.

* Corresponding author. Tel: +358 50 344 2937.
Email address: alp.karakoc@alumni.aalto.fi (Alp Karakoç).

1. INTRODUCTION

Fiber networks, in which the natural or artificial fibers are randomly or directionally aligned and bonded together through chemical, mechanical and/or thermal processes, form the structural foundations of various engineering materials. As seen in Fig. 1, some of these include nonwoven fabrics used in hygiene products, car panels, building and roof coverings, waddings and geotextiles; fiber mats and filters used in electromagnetic shielding and fuel cell gas diffusion layers; sintered metallic fiber networks for prosthetics and metal-matrix composite applications; felted or layered wood fiber networks used in paper and packaging products [1-5]. Their deformation and failure characteristics are dependent on the geometrical and spatial properties of constituent fibers and fiber network connectivity referring to inter-fiber bonds at fiber crossings [6-9].

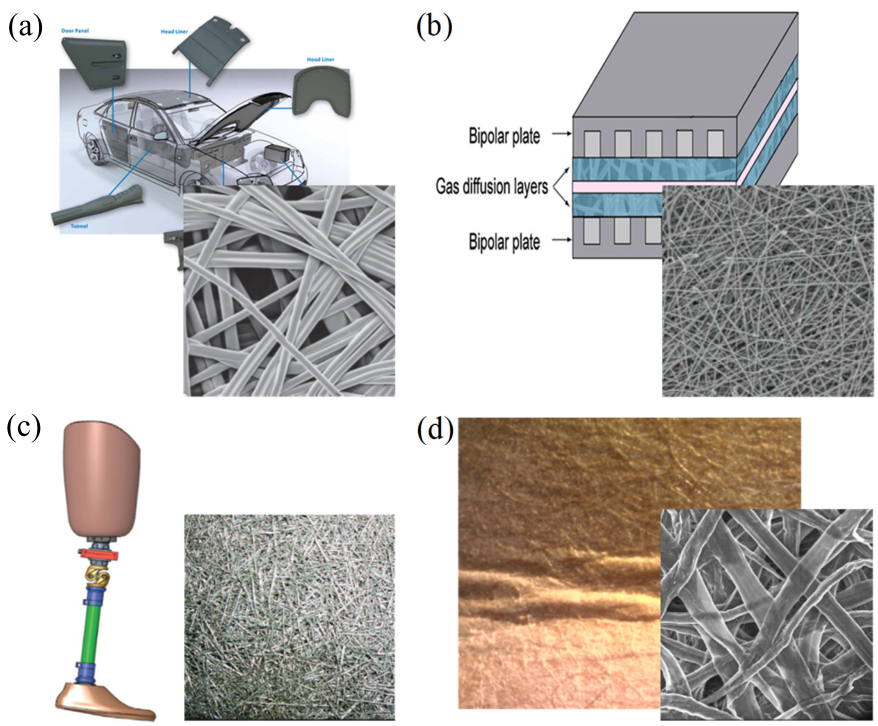

Fig. 1. Various engineering applications and microscope images of their constituents: (a) car panels and nonwoven fabrics [10, 11], (b) fuel cell gas diffusion layers and carbon fiber mats [4, 12], (c) lower-limb prosthesis and sintered metallic fibers in pylon [5, 13], (d) paperboard ply and wood fibers [9, 14].

In order to model fiber network characteristics, various studies have been conducted in which the main strategy is based on continuum or microstructural models. In continuum models, material details and microscopic heterogeneities, e.g. geometrical properties of constituents and their variations, are averaged over the representative volume elements RVEs. The accuracy in continuum models is dependent on the selected RVE size and how well the material details are approximated and represented with these RVEs [15, 16]. Therefore, continuum models are safely used in the analyses for which the material details do not have the highest priority [17]. In microstructural models, geometrical and other physical properties are modeled for each constituent separately, which increases the computational cost. However, it is possible to determine the stresses and strains in each constituent accurately wherein the properties of the material and its constituents can be directly related to each other in microstructural models [18].

Due to direct correlation and accuracy, there have been extensive microstructural modelling investigations on fiber networks in two- and three-dimensional spaces [19-21]. The earliest two dimensional network models were based on random line generation and consolidation in transverse plane. Two dimensional models have been successfully used to determine the in-plane properties where the specimen thickness is of order of one tenth or less of average fiber length and negligible [4, 22]. However, determination of three dimensional properties necessitates an additional dimension, for which the fibers can be deposited and bend on top of each other [23, 24]. Hence, more realistic fiber network structure can be generated with three dimensional models, which also gives a better insight into microstructural properties. However, due to limited computing power in previous decades, it has been a big challenge to create fiber networks mimicking the in-situ conditions in three dimensional space [25, 26].

As a contribution to the previous modelling efforts, a three dimensional statistical microstructural model is introduced so as to analyze the effects of fiber geometry, i.e. length and cross-sectional properties and spatial properties, i.e. location and orientation and specimen size affecting the fiber network connectivity in a statistical manner. By means of the introduced model, a case study on fiber networks forming paper stripe specimens was conducted. The present numerical advancement is believed to guide researchers and designers to investigate fiber network characteristics more efficiently and in shorter time spans.

2. METHODOLOGY

2.1. Geometrical and spatial properties

In the present study, fiber intersections are favored in contrast to the literature studies mainly focusing on short fiber reinforcements and elimination of fiber collision [20, 26-28]. Foundation of the present study follows daily practices such as long fiber reinforced composite materials, paper and paperboards. For this purpose, statistical geometrical model was developed to analyze the effects of geometrical properties of fibers, (i.e. fiber length and cross-sectional properties), and their spatial distribution, (i.e. location and orientation), and specimen dimensions on the fiber network connectivity. Elements of the model consists of geometrical description of fiber, planar projection, fiber trimming and crossing search processes.

As seen in Fig. 2, each individual fiber was described in terms of its spatial properties, i.e. centroid C (X_i, Y_i, Z_i) and $i \in \mathbb{Z}^+$, azimuthal orientation θ and polar orientation ϕ, and geometry, i.e. length l and cross-sectional properties, width w, height h and wall thickness t which was assumed to be same for all cell walls. In addition to this, specimen was described as a rectangular prism with length L, width W and thickness T, which is composed of layers with thickness T_{layer}. In this study, hollow rectangular profile was selected to mimic the wood fiber cross-section composed of cell walls and lumen [29].

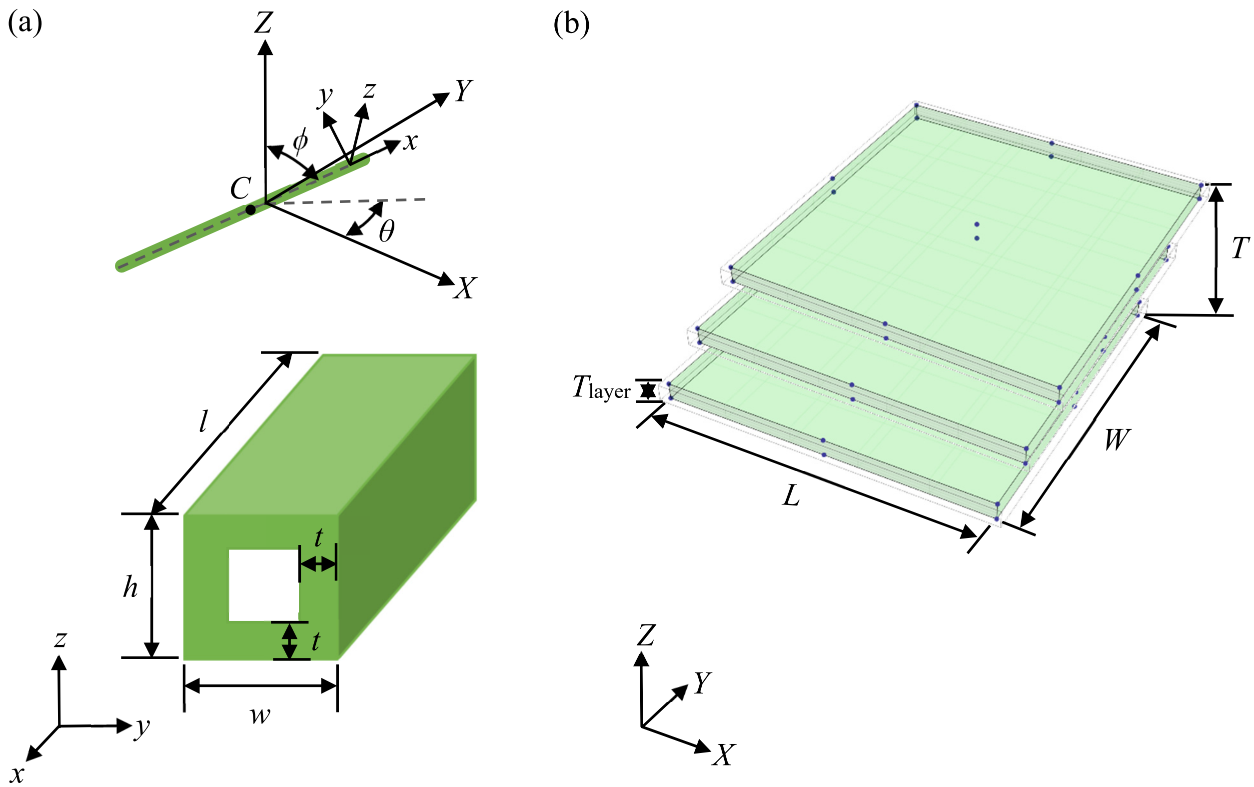

Fig. 2. Fiber profile and distribution: (a) fiber spatial properties in global *XYZ*-Cartesian coordinate system and geometrical properties in local *xyz*-Cartesian coordinate system, (b) layered structure of specimen in global *XYZ*-Cartesian coordinate system.

In order to define the spatial distribution of fibers, fiber centroids were first generated with a uniform probability distribution on a rectangular plane with length L and width W in *XYZ*-Cartesian coordinate system where the Z coordinate of centroids, were kept constant [30]. As seen in Fig. 3, a Monte Carlo type simulation was then used for random selection and picking of each C (X_i, Y_i, Z_i) in an iterative manner. By this way, selection of same fiber centroids was avoided.

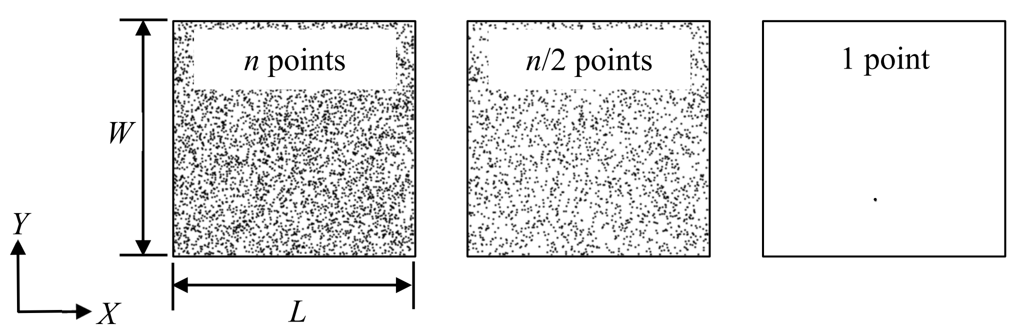

Fig. 3. Schematic representation of Monte-Carlo simulations for random centroid selection.

2.2. Fiber network formation process

Fibers were generated as hollow rectangular prism parallel aligned in the *XY*-plane and deposited into layers of Fig. 2(b) one after another by picking the distributed fiber centroids illustrated in Fig. 3. In order to conduct the deposition process, fiber volume fraction, which is the proportion between the total fiber volume in the confined space $\sum_{f=1}^{n} V_f$ and specimen volume $V = LWT$, was used as the controlling parameter of the iterative deposition algorithm shown in Fig. 4.

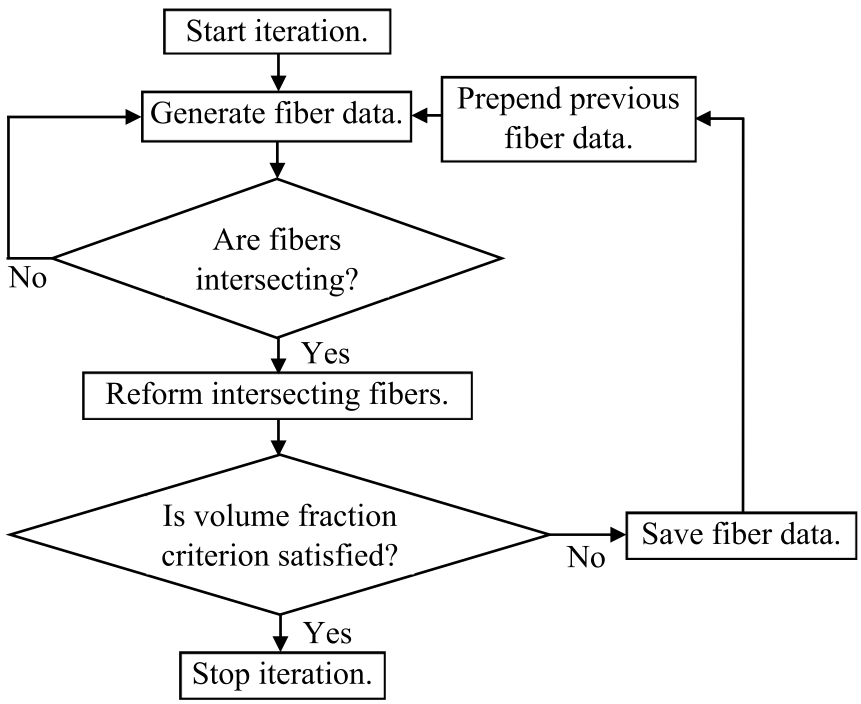

Fig. 4. Fiber deposition algorithm flowchart.

Despite the fiber curvature of in-situ, distance between each fiber crossing were assumed to be close enough so that fiber geometries were taken to be straight for the present investigated fiber network [4]. Thereafter, using the projections in *XY*-plane, fibers exceeding the specimen dimensions L and W in the *XY*-plane were trimmed within the transverse boundaries as seen in Fig. 5 and the fibers out of the boundaries were eliminated, which minimizes boundary artefacts. However, the process ends up with trimming of fibers that are not totally inside the specimen, which was also stated in the literature [1].

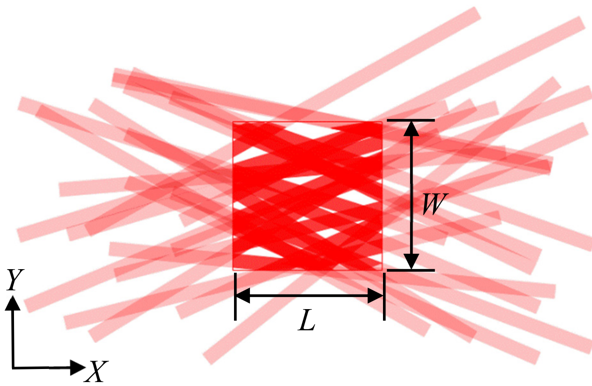

Fig. 5. Cut fibers (dark colored) inside the transverse boundaries.

During the deposition process, XY-planar projection of fibers shown in Fig. 5 were used to detect the possible fiber crossings. In order to detect these crossings, edges of each rectangle were first defined as line segments by using the corner coordinate data. Then, line-to-line intersections were sought among the rectangles, for which a nearest neighboring algorithm was used to confine the region of interest rather than the entire domain and aimed at computational cost reduction. As seen in Fig. 6, the algorithm was based on finding the adjacent fibers partially or totally located inside a disk created using the length l and centroid C (X_i, Y_i, Z_i) of the reference fiber.

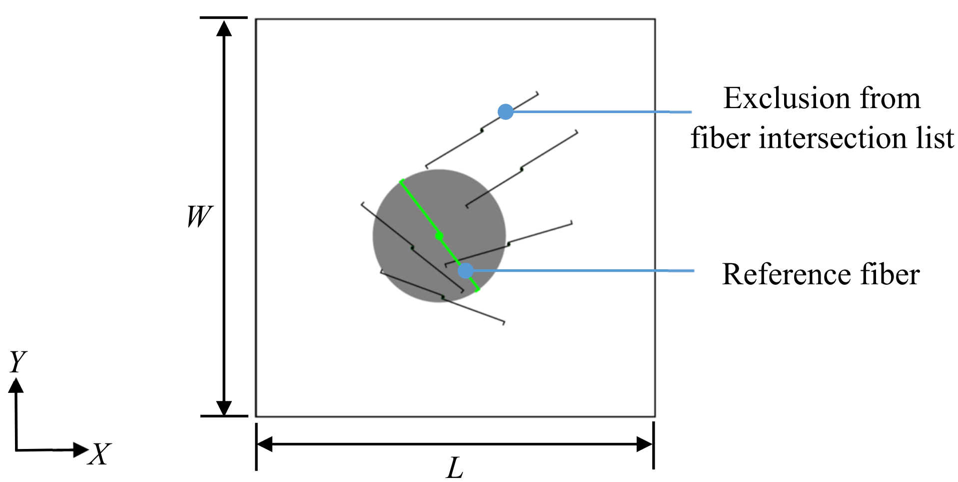

Fig. 6: Crossing detection inside a confined space (gray disk) defined with length l and centroid $C(X_i, Y_i, Z_i)$ of the reference fiber (green line). The fibers partially or totally inside the confined space are used in the crossing detection computations.

As a result of the process, crossings were computed, e.g. resulting in S_1 (x_1, y_1) as seen in Fig. 7(a). By using the azimuthal orientation θ of the deposited fiber in the XY-plane as shown in Fig. 7(a) and flexibility angle φ in XZ-plane as illustrated in Fig. 7(b), side points, e.g. S_2 (x_2, y_2), were generated through

$$\begin{aligned} x_2 &= x_1 - h_{f1} \tan\varphi \cos\theta \\ y_2 &= y_1 - h_{f1} \tan\varphi \sin\theta \end{aligned} \tag{1}$$

in which h_{f1} refers to height of the previously settled fiber. Based on the coordinate data provided through Eq. (1) and height of current fiber h_{f2}, projected rectangles were curved up along Z-axis at the fiber crossings.

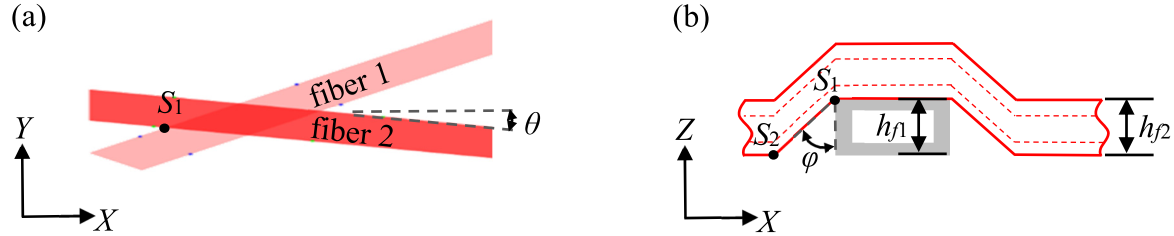

Fig. 7. Fibers and their crossings in two dimensional space: (a) projected view of two fibers (light color represents previously settled one and dark color represents deposited one) and azimuthal orientation θ in the XY-plane, (b) crossing of fiber 1 and fiber 2, and fiber flexibility in terms of flexibility angle φ in XZ-plane.

Curved up fibers were then merged in XYZ-Cartesian coordinate system where number of fiber crossings per fiber n_{cpf} was used as a quantitative parameter for fiber network connectivity. Fig. 8 depicts an example simulation for fibers and their crossings so as to quantify the connectivity.

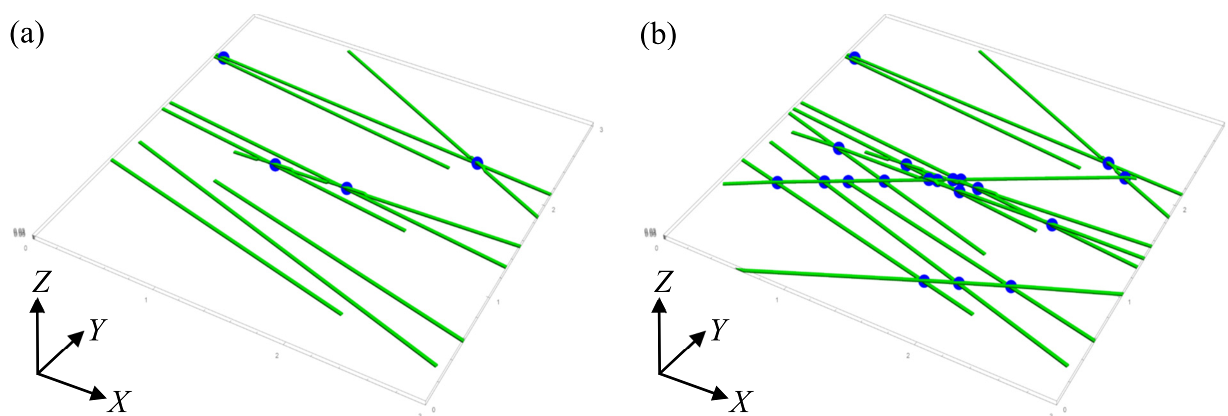

Fig. 8. Fibers and their crossings in three dimensional space: (a) 9 fibers and 4 fiber crossings, (b) 13 fibers and 19 fiber crossings.

In order to obtain in-situ fiber networks, fibers were smoothened by using m^{th} order Bezier curve fitting function $B(v)$ for m+1 (control) points represented with column vector $\mathbf{S}_i$ so that

$$B(v) = \sum_{i=0}^{m} \left\{ \binom{m}{i} v^i (1-v)^{m-1} \right\} \mathbf{S}_i. \tag{2}$$

The row vector in parenthesis is called as Bernstein polynomial basis of order m [31,32]. Being a function with non-dimensional variable $0 \le v \le 1$, $B(v)$ of Eq. (2) eliminates the lower and upper limit calculations in *XYZ*-Cartesian coordinate system and is applicable to set of points in two and three dimensional spaces.

For increasing or decreasing the smoothing effect, fibers were discretized with a segmentation function that is also based on Eq. (2). This function modifies the size of column vector $\mathbf{S}_i$, thus the polynomial order n, by adding and removing points between each initially generated consecutive points. Fig. 9 illustrates the implemented segmentation and Bezier curve fitting functions.

(a) 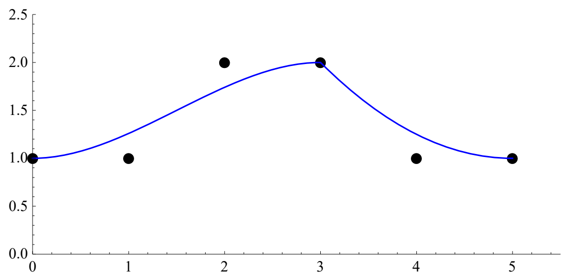

(b) 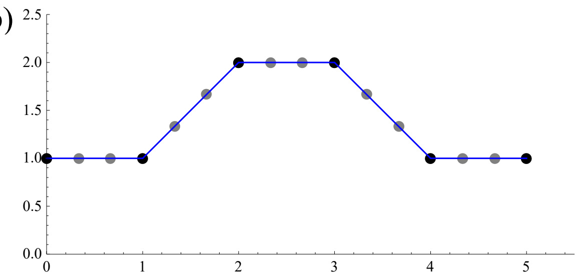

Fig. 9. Segmentation and curve fitting: (a) initially generated (control) points and curves with Bezier curve fitting function, (b) added (control) points and curve segments formed with Bezier curve fitting function. Here, black and gray points represent the initially generated and added points, respectively whereas the line represents the Bezier curve.

In regard to computational costs and realistic representation of the fibers, 4 points (forming 5 segments) were added between each initially generated consecutive points (please, see Fig. 9(a)). The smoothed fibers were then used to mimic the in-situ fibers as seen in Fig. 10.

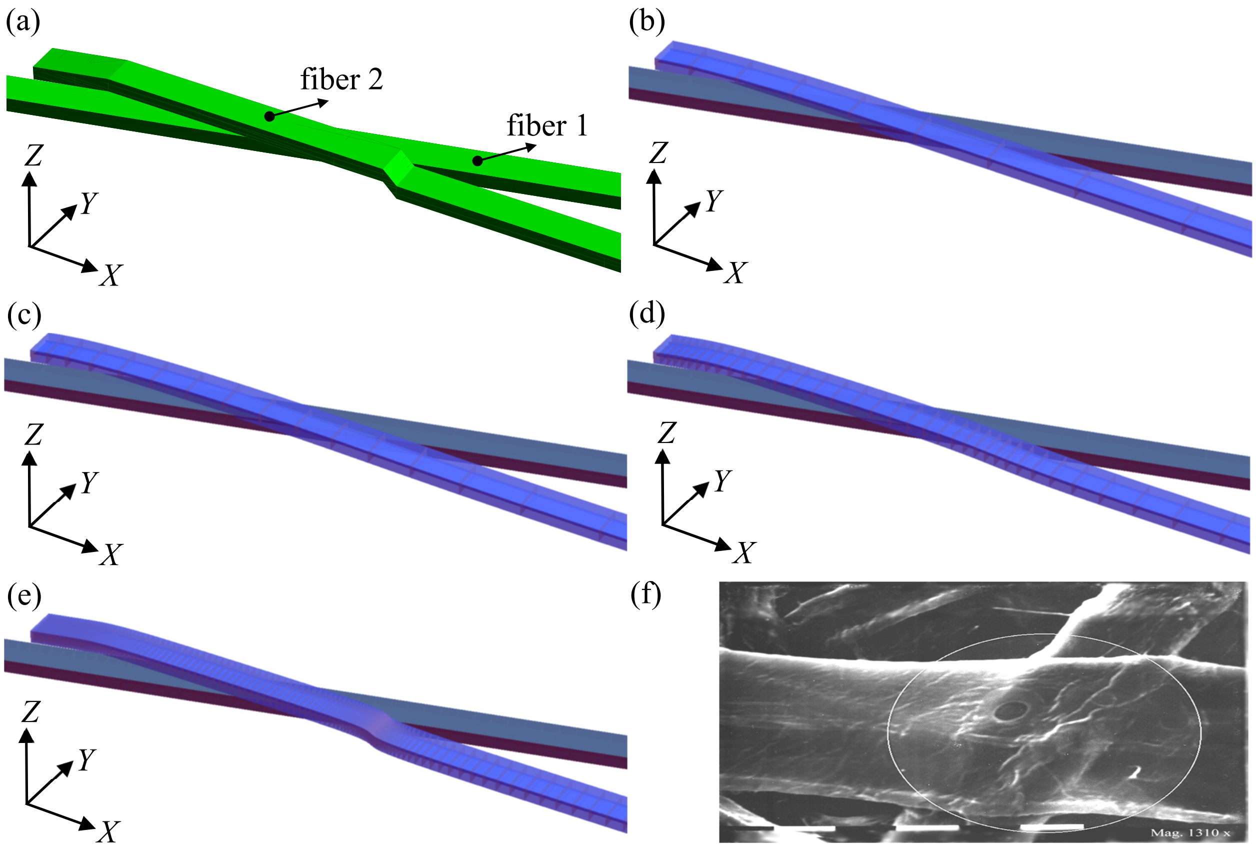

Fig. 10. Fiber smoothing by means of segmentations *XYZ*-Cartesian coordinate system for mimicking fibers in-situ: (a) fiber before smoothing effect; (b) 1 segment, (c) 2 segments, (d) 5 segments, (e) 20 segments between consecutive points, (f) fiber crossing microscopic view.

As a result of this process, specimens were formed, some of which are shown in Fig. 11.

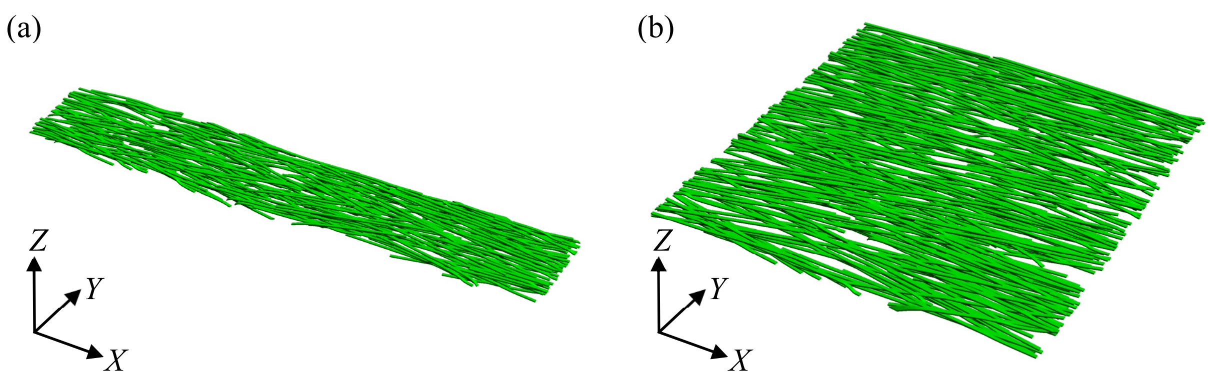

Fig. 11. Specimens with their characteristics geometrical parameters: (a) rectangular specimen, (b) square specimen.

3. RESULTS AND DISCUSSION

The present simulation experiments were designed so that selected fiber lengths and cross-sectional properties, flexibility angles and specimen sizes were in accordance with previous paper and paperboard investigations in the literature [1, 9, 23, 24, 33, 34]. Layer thickness was taken as T_{layer}=0.020 mm for each specimen, fiber wall thickness was assumed to be t=0.004 mm and polar orientation was approximated as ϕ=0° because of the formation characteristics of paper stripe specimens [35]. After reaching the designated fiber volume fraction of 40% for a layer, fibers were deposited onto the upper layer so as to mimic the layered structure of investigated material.

3.1. Effects of fiber geometry on fiber network connectivity

In order to understand how the fiber geometry affects the fiber network connectivity, simulation experiments were conducted with n_s=3 repetitions for each set listed in Table 1. In these experiments, azimuthal orientation was taken to be θ=0° and its variation $\Delta\theta$ was in the range of ±15° based on the machine-made paper data provided in the literature [35]. Specimen dimensions were taken to be length L=5 mm, width W=1 mm and thickness T=0.060 mm mimicking paper stripe specimens [24].

Table 1. Design of experiments based on fiber geometrical parameters.

	Set	Untrimmed fiber length l (mm)	Fiber width w (mm)	Fiber height h (mm)	Flexibility angle φ (°)
Fiber length l	1	1.0	0.025	0.010	30
	2	1.5	0.025	0.010	30
	3	2.0	0.025	0.010	30
Fiber width w	4	2.0	0.020	0.010	30
	5	2.0	0.025	0.010	30
	6	2.0	0.030	0.010	30
Fiber height h	7	2.0	0.025	0.005	30
	8	2.0	0.025	0.010	30
	9	2.0	0.025	0.020	30
Fiber flexibility angle φ	10	2.0	0.025	0.010	15
	11	2.0	0.025	0.010	30
	12	2.0	0.025	0.010	45

Because of simulation results being positive and non-symmetric, lognormal distribution was selected for expressing the continuous probability distribution of the number of crossings per fiber n_{cpf} subject to the investigated geometrical parameter, which can be expressed as

$$P(n_{\mathrm{cpf}}) = \frac{\exp\left(-\frac{\left(-\mu_{\mathrm{d}} + \ln(n_{\mathrm{cpf}})\right)^2}{2\sigma_{\mathrm{d}}^{\;2}} \right)}{\sqrt{2\pi}\, n_{\mathrm{cpf}}\, \sigma_{\mathrm{d}}}. \tag{3}$$

Here, π is the mathematical constant taken as 3.14159, exp refers to the exponential function, ln is the natural logarithm while μ_{d} and σ_{d} are the mean and standard deviation of the continuous probability distribution, which were taken as first order (linear) polynomial functions of the tested geometrical parameter, so called variable v, i.e. $\underline{\mu}_{\mathrm{d}}(v)$ and $\underline{\sigma}_{\mathrm{d}}(v)$. Hence, it was possible to fit the simulation results by means of Eq. (3) and estimate the distribution subject to v. For example, being fiber length l as the variable v, estimated probability distribution for the number of crossings per fiber n_{cpf} follows

$$\underline{P}(n_{\mathrm{cpf}}, l) = \frac{\exp\left(-\frac{\left(-\underline{\mu}_{\mathrm{d}}(l) + \ln(n_{\mathrm{cpf}})\right)^2}{2\left(\underline{\sigma}_{\mathrm{d}}(l)\right)^2} \right)}{\sqrt{2\pi}\, n_{\mathrm{cpf}}\, \underline{\sigma}_{\mathrm{d}}(l)}. \tag{4}$$

Fig. 12 shows the fitted and estimated distributions via Eqs. (3) and (4), which are based on number of crossing per fiber n_{cpf} for fiber lengths l={1, 1.5, 2} mm. It can be deduced from Fig. 12 and Table 2 that both the distribution extremum and maximum values for n_{cpf} are positively affected with l. This is valid due to increasing likelihood of fiber crossings with l. Another interesting outcome is the increase in uncertainty near the probability distribution extremum, which is described as $\mu_{\mathrm{s}} \pm \sigma_{\mathrm{s}} / n_{\mathrm{s}}^{0.5}$ where μ_{s}, σ_{s} are the mean and standard deviation of n_{cpf} distribution probabilities obtained from simulations after n_{s} repetition.

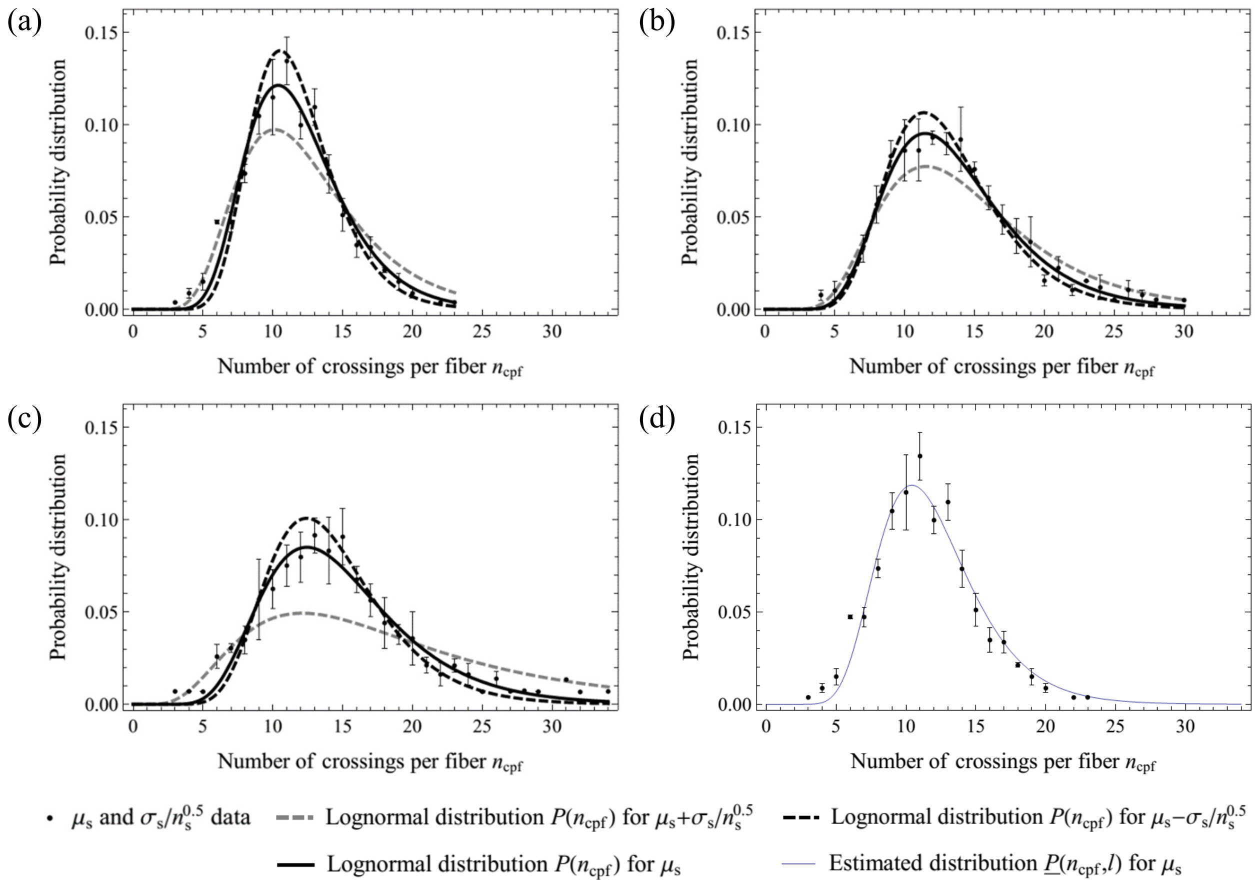

Fig. 12. Probability distributions for number of crossings per fiber n_{cpf}: (a) l=1 mm, (b) l=2 mm, (c) l=3 mm, (d) estimated probability distribution $\underline{P}(n_{cpf},l)$ for the mean data μ_s obtained from the simulations for l=1 mm. The whiskers represents the data range obtained after n_s=3 repetitions.

Table 2. The highest probability distributions and maximum values for number of crossing per fiber n_{cpf}, and estimated distributions within the limits of the investigated parameter.

	Set	(mm)	max(μ_s) → n_{cpf}	max(n_{cpf})	$\underline{P}(n_{cpf},l)$
l	1	1.0	0.159 → 11	23	$\frac{7.69\exp\left(-\frac{(-0.21l+\log(n_{cpf})-2.22)^2}{2(0.05l+0.26)^2}\right)}{(l+4.93)\,n_{cpf}}$
	2	1.5	0.121 → 14	30	
	3	2.0	0.119 → 15	34	

In contrast to l, fiber width w has a negative effect on the fiber connectivity. The main reason is the volumetric increase in fibers and hence decrease in number of fibers in the confined volume. As seen in Fig. 13(a)-(b) and Table 3, this leads to decreasing probability of fiber crossings and maximum n_{cpf}. Similar to w, increase in fiber height h causes a decrease in the number of fibers inside the specimen. Hence, increase in h has a negative impact on the distribution extremum and maximum values for n_{cpf} as also deduced from Fig. 13(c)-(d) and Table 3. Similar trend was observed for the effect of flexibility angle φ investigations on the distribution extremum and maximum values of n_{cpf}. As also proved in the literature, it is principally related to increase in fiber packing probability. However, increase in fiber flexibility, i.e. small values of φ, may result in fiber networks that do not resemble the real material structure [25].

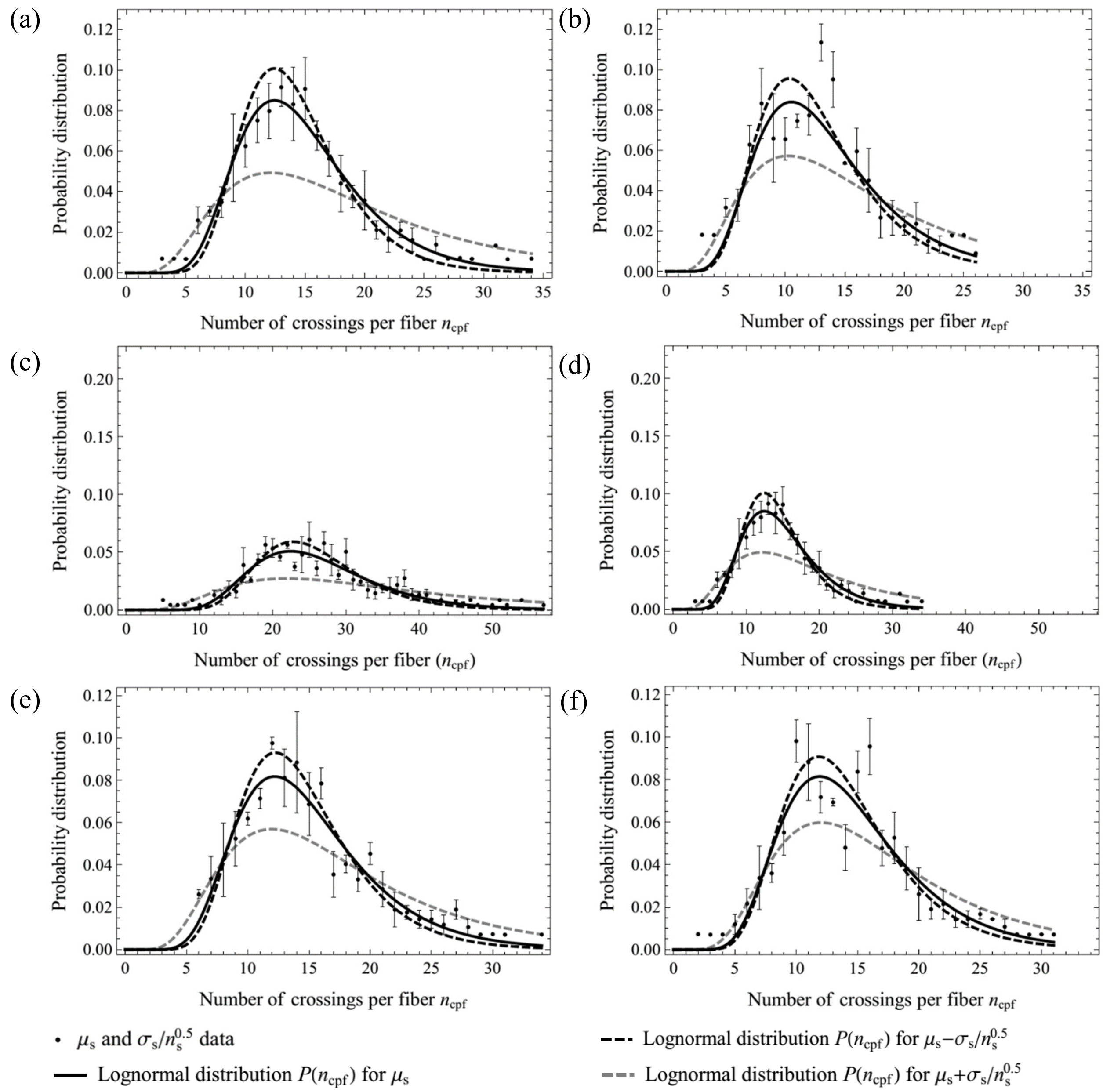

Fig. 13. Probability distributions for number of crossings per fiber n_{cpf}: (a) w= 0.025 mm, (b) w= 0.030 mm, (c) h=0.005 mm, (d) h=0.010 mm, (e) φ= 15°, (f) φ= 45°. The whiskers represents the data range obtained after n_s=3 repetitions.

Table 3. The highest probability distributions and maximum values for number of crossing per fiber n_{cpf}, and estimated distributions within the limits of the investigated parameter

	Set	(mm)	$\max(\mu_s) \rightarrow n_{\mathrm{cpf}}$	$\max(n_{\mathrm{cpf}})$	$\underline{P}(n_{\mathrm{cpf}}, w)$
w	4	0.020	0.118 → 16	35	$\dfrac{0.06\exp\left(-\dfrac{(16.39\,w+\log(n_{\mathrm{cpf}})-3.03)^2}{2(7.02\,w+0.19)^2}\right)}{(w+0.028)\,n_{\mathrm{cpf}}}$
	5	0.025	0.119 → 15	34	
	6	0.030	0.127 → 13	26	
	Set	(mm)	$\max(\mu_s) \rightarrow n_{\mathrm{cpf}}$	$\max(n_{\mathrm{cpf}})$	$\underline{P}(n_{\mathrm{cpf}}, h)$
h	7	0.005	0.088 → 25	57	$\dfrac{0.09\exp\left(-\dfrac{(90.84\,h+\log(n_{\mathrm{cpf}})-3.63)^2}{2(4.63\,h+0.31)^2}\right)}{(h+0.07)\,n_{\mathrm{cpf}}}$
	8	0.010	0.119 → 15	34	
	9	0.020	0.221 → 7	20	
	Set	(°)	$\max(\mu_s) \rightarrow n_{\mathrm{cpf}}$	$\max(n_{\mathrm{cpf}})$	$\underline{P}(n_{\mathrm{cpf}}, \varphi)$
φ	10	15	0.121 → 16	34	$\dfrac{1288.65\exp\left(-\dfrac{(0.0005\,\varphi+\log(n_{\mathrm{cpf}})-2.65)^2}{2(0.0003\,\varphi+0.36)^2}\right)}{(\varphi+1163.97)\,n_{\mathrm{cpf}}}$
	11	30	0.119 → 15	34	
	12	45	0.121 → 14	31	

3.2. Effects of specimen size and orientation on fiber network connectivity

In order to understand how specimen size and orientation affect fiber network connectivity, simulation experiments were conducted with n_s=3 repetitions for each set listed in Table 4. In these experiments, geometrical properties of fibers were taken to be length l=2 mm, width w=0.025 mm, height h=0.010 mm, thickness t=0.004 mm with flexibility angle φ=30°.

Table 4. Design of experiments based on specimen size and orientation.

	Set	Azimuthal orientation variation $\Delta\theta$ (°) (with θ=0°)	Specimen length L (mm)	Specimen width W (mm)	Specimen thickness T (mm)
Azimuthal orientation variation $\Delta\theta$	13	± 0	5.0	1.0	0.060
	14	± 15	5.0	1.0	0.060
	15	± 30	5.0	1.0	0.060
Specimen length L (and width W)	16	± 15	2.0	2.0	0.060
	17	± 15	3.0	3.0	0.060
	18	± 15	5.0	5.0	0.060
Specimen thickness T	19	± 15	5.0	1.0	0.060
	20	± 15	5.0	1.0	0.080
	21	± 15	5.0	1.0	0.100

The azimuthal orientation θ and especially its variation $\Delta\theta$ of the deposited fiber in the *XY*-plane are important investigation parameters since the effective properties are highly influenced by the fiber orientation distribution. The azimuthal orientation distribution is inherited from the fiber deposition process and can be partially controlled by manufacturing process, e.g. fiber alignment in machine and cross directions during paper formation [36]. As deduced from Fig. 14(a)-(b), increase in $\Delta\theta$ favors number of fiber crossings per fiber n_{cpf} and uniform distribution. The results also give an insight into the decrease of material directional properties with increase in $\Delta\theta$.

Similar to the effect of $\Delta\theta$, a positive relation exists in consideration to specimen length L and width W. As seen in Fig. 14(c)-(d) and Table 5, both the distribution extremum and maximum values for n_{cpf} are positively affected with increase in L (or W). The results are in good agreement with the findings of previous investigations by providing a microstructural explanation to so called "scale effect", which addresses the heterogeneities of fiber networks on different material scales [37-39]. In addition to the abovementioned parameters and their effects, a positive influence on n_{cpf} can be observed with increase in specimen thickness T, which is shown in Fig. 14(e)-(f) and Table 5. Since the volume fraction is same for each specimen, number of fibers and n_{cpf} increase with T.

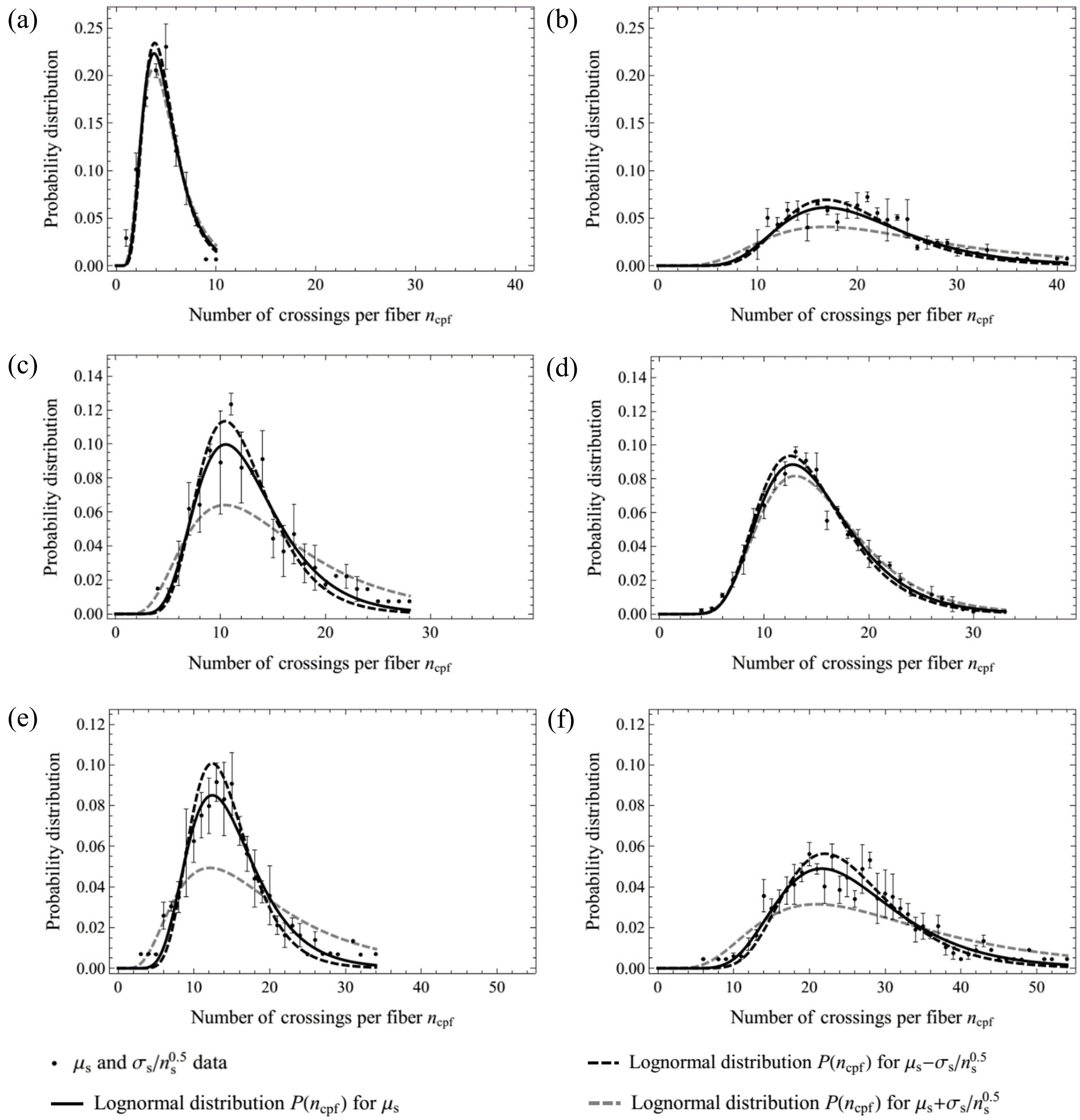

Fig. 14. Probability distributions for number of crossings per fiber n_{cpf}: (a) $\Delta\theta$ =± 0°, (b) $\Delta\theta$ =± 30°, (c) L =2.0 mm and W =2.0 mm, (d) L =3.0 mm and W =3.0 mm, (e) T = 0.06 mm, (f) T = 0.10 mm. The whiskers represents the data range obtained after n_s=3 repetitions.

Table 5. The highest probability distributions and maximum values for number of crossing per fiber n_{cpf}, and estimated distributions win the limits of the investigated parameter.

	Set	(°)	$\max(\mu_s) \rightarrow n_{cpf}$	$\max(n_{cpf})$	$\underline{P}(n_{cpf}, \Delta\theta)$
$\Delta\theta$	13	± 0	0.267 → 5	10	$\dfrac{179.21\exp\left(-\dfrac{(-0.05\Delta\theta+\log(n_{cpf})-1.65)^2}{2(0.42-0.002\,\Delta\theta)^2}\right)}{(186.61-\Delta\theta)\,n_{cpf}}$
	14	± 15	0.119 → 15	34	
	15	± 30	0.09 → 20	41	
	Set	(mm)	$\max(\mu_s) \rightarrow n_{cpf}$	$\max(n_{cpf})$	$\underline{P}(n_{cpf}, L)$
L	16	2.0	0.149 → 10	28	$\dfrac{70.26\exp\left(-\dfrac{(-0.04\,L+\log(n_{cpf})-2.36)^2}{2(0.38-0.0056782\,L)^2}\right)}{(67.64-L)\,n_{cpf}}$
	17	3.0	0.110 → 12	33	
	18	5.0	0.105 → 15	39	
	Set	(mm)	$\max(\mu_s) \rightarrow n_{cpf}$	$\max(n_{cpf})$	$\underline{P}(n_{cpf}, T)$
T	19	0.060	0.119 → 15	34	$\dfrac{20.78\exp\left(-\dfrac{(-13.84\,T+\log(n_{cpf})-1.83)^2}{2(0.36-0.02\,T)^2}\right)}{(18.84-T)\,n_{cpf}}$
	20	0.080	0.119 → 20	41	
	21	0.100	0.068 → 27	54	

4. CONCLUSIONS

In the current study, a three dimensional statistical microstructural model is introduced so as to analyze the effects of fiber geometry, i.e. length and cross-sectional properties and spatial properties, i.e. location and orientation and specimen size affecting the fiber network connectivity in a statistical manner. By means of the introduced model, a case study on fiber networks forming paper and packaging products was conducted. The results were represented in terms of probability distribution functions showing the relation between the studied geometrical parameters and the number of crossings per fiber n_{cpf}, which can be used as a quantitative representation of the fiber network connectivity.

The compact statistical description for each parametric relation was given by means of lognormal distribution, the choice of which was due to the simulation results being positive and non-symmetric. As a result of the parametric relations, it was deduced that fiber geometrical parameters, fiber orientation and specimen size have great impact on the fiber network connectivity, which also affects the mechanical characteristics of the material. Fiber geometry analysis on connectivity shows that both the distribution extremum and maximum values for n_{cpf}

are positively affected by fiber length l, which is due to increasing likelihood of fiber crossings. However, fiber width w has a negative effect because of the volumetric increase in fibers and hence decrease in number of fibers in the confined volume. For the same reason with w, fiber height h also has negative effect on the fiber network connectivity. Similar trend was observed for the effect of flexibility angle φ investigations on the distribution extremum and maximum value of n_{cpf}. As also proved in the literature, it is principally related to increase in fiber packing probability. However, increase in fiber flexibility, i.e. small values of φ, may result in fiber networks that do not resemble the real material structure. In addition to this, specimen geometry analysis shows that the azimuthal orientation variation $\Delta\theta$, specimen length L, width W and thickness T have positive impacts on the connectivity. The increase in $\Delta\theta$ results in higher probabilities of fiber intersections in the investigated plane and orientation variation range. On the other hand, the positive impacts of L, W and T can be directly related to the increasing probabilities of fiber connectivity with volume changes, which also supports the so called "scale effect" and address the heterogeneities of fiber networks on different material scales.

Eventually, the current simulation methodology and tool, a sample Mathematica code of which is also provided in Appendix A, and the probability distribution functions that are ready-to-use are believed to be beneficial for researchers and designers in characterization of fibrous materials such as nonwoven textiles, paper and packaging products.

ACKNOWLEDGMENTS

The authors gratefully acknowledge the supports of Aalto University-PuuPostdoc research fund, and Tekniikan edistämissäätiö TES through Foundations' Post Doc Pool, Finland.

REFERENCES

1. Kulachenko A, Uesaka T. Direct simulations of fiber network deformation and failure. Mechanics of Materials 2012; 51(0): 1-14.

2. Iorga L, Pan Y, Pelegri A. Numerical characterization of material elastic properties for random fiber composites. Mechanics of Materials and Structures 2008/9/1; 3(7): 1279-1298.

3. Russell S. Handbook of Nonwovens. Boca Raton, Florida, USA.: The Textile Institute: Woodhead Publishing Ltd, CRC Press, 2007.

4. Sampson W. Modelling Stochastic Fibrous Materials with Mathematica. Springer-Verlag London, 2009.

5. Veyhl C, Fiedler T, Jehring U, Andersen O, Bernthaler T, Belova IV, Murch GE. On the mechanical properties of sintered metallic fibre structures. Materials Science and Engineering: A 2013; 562(0): 83-88.

6. Jin BC. 3-D numerical simulation and analysis of complex fiber geometry RaFC materials with high volume fraction and high aspect ratio based on Abaqus Python. Master's thesis, 2011. Rutgers, The State University of New Jersey.

7. Pan Y. Stiffness and progressive damage analysis on random chopped fiber composite using FEM. Doctoral thesis, 2010. Rutgers, The State University of New Jersey.

8. Curto JMR, Conceição ELT, Portugal ATG, Simoes RMS. The fibre properties influence on a three dimensional paper model. XXI Tecnicelpa Conference and Exhibition 2010.

9. Alava MJ, Niskanen K. The physics of paper. Reports on progress in physics 2006; 69: 669-723.

10. Isover. http://www.isover-technical-insulation.com/var/technicalinsulation/storage/images/oem-insulation/cars-trucks/presentation/cars-insulation-solutions/123087-1-eng-GB/Cars-insulation-solutions_reference.png.; 2015 (April).

11. Ridruejo A, Jubera R, González C, LLorca J. Inverse notch sensitivity: Cracks can make nonwoven fabrics stronger. J Mech Phys Solids 2015; 77(0): 61-69.

12. Bazylak A, Berejnov V, Markicevic B, Sinton D, Djilali N. Numerical and microfluidic pore networks: Towards designs for directed water transport in GDLs. Electrochim Acta 2008; 53(26): 7630-7637.

13. Kobayashi T, Orendurff MS, Boone DA. Effect of alignment changes on socket reaction moments during gait in transfemoral and knee-disarticulation prostheses: Case series. J Biomech 2013; 46(14): 2539-2545.

14. Huang H, Hagman A, Nygårds M. Quasi static analysis of creasing and folding for three paperboards. Mechanics of Materials 2014; 69(1): 11-34.

15. Freund J, Karakoç A, Sjölund J. Computational homogenization of regular cellular material according to classical elasticity. Mechanics of Materials 2014; 78: 56-65.

16. Karakoç A, Freund J. A direct simulation method for the effective in-plane stiffness of cellular materials. International Journal of Applied Mechanics 2013; 5 (03): 1350034

17. Mark A, Svenning E, Rundqvist R, Edelvik F, Glatt E, Rief S, Wiegmann A, Fredlund M, Lai R, Martinsson L, Nyman U. Microstructure Simulation of Early Paper Forming Using Immersed Boundary Methods. Tappi journal 2011; 10(11): 23-30.

18. Farukh F, Demirci E, Ali H, Acar M, Pourdeyhimi B, Silberschmidt V. Nonwovens modelling: a review of finite-element strategies. The Journal of The Textile Institute 2015; 4:1-8.

19. Curto JMR, Conceição ELT, Portugal ATG, Simões RMS. Three dimensional modelling of fibrous materials and experimental validation; Dreidimensionale Modellierung von Fasermaterialien und experimentelle Validierung. Materialwissenschaft und Werkstofftechnik 2011; 42(5): 370-374.

20. Abd El-Rahman, Ahmed I. A1Tucker, III,Charles L. Mechanics of Random Discontinuous Long-Fiber Thermoplastics—Part I: Generation and Characterization of Initial Geometry. Journal of Applied Mechanics 2013; 80(5): 051007-051007.

21. Provatas N, Haataja M, Asikainen J, Majaniemi S, Alava MJ, Nissila AT. Fiber deposition models in two and three spatial dimensions. Colloids and Surfaces A 2000; 165: 209-229.

22. Sampson W, The structural characterisation of fibre networks in papermaking processes - a review. In: 11th Fundamental Research Symposium. Manchester 2001: 1205.

23. Lavrykov S, Singh KM, Ramarao BV, Elasticity and stiffness of paper: a model based study of the influence of fibers. In: Progress in Paper Physics Seminar 2011; 35-40.

24. Lavrykov S, Lindström SB, Singh KM, Ramarao BV. 3D network simulations of paper structure. Nordic Pulp Paper Research Journal 2012; 27(2): 256-263.

25. Kulachenko A, Denoyelle T, Galland S, Lindström SB. Elastic properties of cellulose nanopaper. Cellulose 2012; 19(3): 793-807.

26. Pan Y, Iorga L, Pelegri AA. Numerical generation of a random chopped fiber composite RVE and its elastic properties. Composites Sci Technol 2008; 68(13): 2792-2798.

27. Pan Y, Iorga L, Pelegri AA. Analysis of 3D random chopped fiber reinforced composites using FEM and random sequential adsorption. Computational Materials Science 2008; 43(3): 450-461.

28. Conceicao ELT, Curto JMR, Simões RMS, A.T.G. A. Coding a simulation model of the 3D structure of paper. CompIMAGE 2010: 299-310.

29. Torgnysdotter A, Kulachenko A, Gradin P, Wågberg L. Fiber/Fiber Crosses: Finite Element Modeling and Comparison with Experiment. Journal of Composite Materials 2007; 41(13): 1603-1618.

30. Karakoc A, Freund J. Statistical strength analysis for honeycomb materials. International Journal of Applied Mechanics 2013; 02.

31. Lu L. Explicit algorithms for multiwise merging of Bézier curves. J Comput Appl Math 2015;278(0): 138-148.

32. Muraru CV. On a problem of fitting data using Bezier Curves. Brain Broad Research in Artificial Intelligence and Neuroscience 2010; 1(2): 127-132.

33. Hakkila P, Verkasalo E. Structure and properties of wood and woody biomass. In: Kellomäki S, editor. Forest Resources and Sustainable Management. : Published in cooperation with the Finnish Paper Engineers' Association and TAPPI, 2009; 133-215.

34. Bronkhorst CA. Modelling paper as a two-dimensional elastic-plastic stochastic network. International Journal of Solids and Structures 2003;40:5441-5454.

35. Niskanen K. Paper Physics. Finland: Fapet Oy, 1998.

36. Cox HL. The elasticity and strength of paper and other fibrous materials. British Jounal of Applied Physics 1952; 3: 72-79.

37. Karakoç A, Freund J. A statistical failure initiation model for honeycomb materials. Composite Structures 2013; 95(0): 154-162.

38. Lee Y, Jasiuk I. Apparent elastic properties of random fiber networks. Computational Materials Science 2013; 79(0): 715-723.

39. Shahsavari AS, Picu RC. Size effect on mechanical behavior of random fiber networks. Int J Solids Structures 2013; 50(20–21): 3332-3338.

APPENDIX A: SUPPLEMENTARY MATERIAL

Sample Mathematica code for generating layered fiber network in a rectangular domain is provided with predefined parameters in its user interface as supplementary material.